frontiers in Immunology

ORIGINAL RESEARCH
published: 22 March 2022
doi: 10.3389/fimmu.2022.853572

In-Depth Immunophenotyping With Mass Cytometry During TB Treatment Reveals New T-Cell Subsets Associated With Culture Conversion

Carole Chedid[1,2,3‡], Thibault Andrieu[4], Eka Kokhreidze[5‡], Nestani Tukvadze[5‡], Samanta Biswas[6‡], Md. Fahim Ather[6‡], Mohammad Khaja Mafij Uddin[6‡], Sayera Banu[6‡], Flavio De Maio[7], Giovanni Delogu[7], Hubert Endtz[2‡], Delia Goletti[8], Marc Vocanson[1], Oana Dumitrescu[1,9,10], Jonathan Hoffmann[1,2†‡] and Florence Ader[1,11†]*

[1] Centre International de Recherche en Infectiologie, Legionella Pathogenesis Group, INSERM U1111, Université Claude Bernard Lyon 1, CNRS UMR5308, École Normale Supérieure de Lyon, Lyon, France, [2] Medical and Scientific Department, Fondation Mérieux, Lyon, France, [3] Département de Biologie, Ecole Normale Supérieure de Lyon, Lyon, France, [4] Cytometry Core Facility, Centre de Recherche en Cancérologie de Lyon, Université Claude Bernard Lyon 1, Inserm 1052, CNRS 5286, Centre Léon Bérard, Lyon, France, [5] National Center for Tuberculosis and Lung Diseases (NCTBLD), Tbilisi, Georgia, [6] Infectious Diseases Division, International Centre for Diarrhoeal Disease Research, Bangladesh (icddr,b), Dhaka, Bangladesh, [7] Dipartimento di Scienze biotecnologiche di base, cliniche intensivologiche e perioperatorie – Sezione di Microbiologia, Università Cattolica del Sacro Cuore, Rome, Italy, [8] Department of Epidemiology and Preclinical Research, "L. Spallanzani" National Institute for Infectious Diseases-IRCCS, Rome, Italy, [9] Hospices Civils de Lyon, Institut des Agents Infectieux, Laboratoire de Bactériologie, Lyon, France, [10] Université Lyon 1, Facultés de Médecine et de Pharmacie de Lyon, Lyon, France, [11] Hospices Civils de Lyon, Hôpital de la Croix-Rousse, Département des Maladies Infectieuses et Tropicales, Lyon, France

Tuberculosis (TB) is a difficult-to-treat infection because of multidrug regimen requirements based on drug susceptibility profiles and treatment observance issues. TB cure is defined by mycobacterial sterilization, technically complex to systematically assess. We hypothesized that microbiological outcome was associated with stage-specific immune changes in peripheral whole blood during TB treatment. The T-cell phenotypes of treated TB patients were prospectively characterized in a blinded fashion using mass cytometry after *Mycobacterium tuberculosis* (*Mtb*) antigen stimulation with QuantiFERON-TB Gold Plus, and then correlated to sputum culture status. At two months of treatment, cytotoxic and terminally differentiated $CD8^+$ T-cells were under-represented and naïve $CD4^+$ T-cells were over-represented in positive- *versus* negative-sputum culture patients, regardless of *Mtb* drug susceptibility. At treatment completion, a T-cell immune shift towards differentiated subpopulations was associated with TB cure. Overall, we identified specific T-cell profiles associated with slow sputum converters, which brings new insights in TB prognostic biomarker research designed for clinical application.

Keywords: tuberculosis, T-cell, mass cytometry (CyTOF), unsupervised analysis, immunomonitoring

OPEN ACCESS

Edited by:
Katalin A. Wilkinson, Francis Crick Institute, United Kingdom

Reviewed by:
Virginie Rozot, South African Tuberculosis Vaccine Initiative (SATVI), South Africa
Sara Suliman, Brigham and Women's Hospital and Harvard Medical School, United States

***Correspondence:**
Carole Chedid
carole.ched@gmail.com

[†]*These authors share senior authorship*

[‡]*On behalf of the HINTT working group within the GABRIEL network*

Specialty section:
This article was submitted to Microbial Immunology, a section of the journal Frontiers in Immunology

Received: *12 January 2022*
Accepted: *22 February 2022*
Published: *22 March 2022*

Citation:
Chedid C, Andrieu T, Kokhreidze E, Tukvadze N, Biswas S, Ather MF, Uddin MKM, Banu S, De Maio F, Delogu G, Endtz H, Goletti D, Vocanson M, Dumitrescu O, Hoffmann J and Ader F (2022) In-Depth Immunophenotyping With Mass Cytometry During TB Treatment Reveals New T-Cell Subsets Associated With Culture Conversion. Front. Immunol. 13:853572. doi: 10.3389/fimmu.2022.853572

INTRODUCTION

Tuberculosis (TB) is one of the leading causes of death of infectious origin, responsible for 1.5 million deaths worldwide in 2020 (1). TB treatment regimens have toxic side effects (2) requiring monitoring throughout treatment to adapt it and assess effectiveness. Pulmonary TB treatment monitoring relies on *Mycobacterium tuberculosis* (*Mtb*) detection in sputum samples (3), which can be difficult to collect in later stages of treatment (4). Smear microscopy yields highly sample- and operator-dependent results and has poor sensitivity (5). Sputum culture is the gold standard, although slow and requiring biosafety laboratory environments (6). Simultaneously, one of the main stakes in improving TB management is shortening TB treatment (7). Overall, there is a need for novel non-sputum-based tools to monitor disease resolution and assess cure while remaining feasible in primary care settings (8). Blood-based host immune biomarkers have recently gained interest in TB research as immune cells undergo phenotypic changes throughout the disease. Numerous past investigations have pointed to variations in the abundance and marker expression of several targeted subpopulations (9–12), in particular T-cells, which are associated with for *Mtb* clearance (13). While this topic has been addressed in a high-dimensional fashion by transcriptomics studies in high-TB prevalence areas (14–16), cytometry studies directly measuring these cell subpopulation abundance variations have been performed mostly in low-TB prevalence settings or with conventional flow cytometry, targeting a limited number of cell markers (17, 18).

High-dimensional single-cell technologies such as mass cytometry enable the detection and quantification of a high number of cell markers (19). This technique bypasses the limitations of spectral overlap by using monoclonal antibodies coupled to metal polymers, and has allowed high-dimensional exploration of the immune landscape in several domains (20, 21). It has been applied to immune profiling during TB treatment in a 2018 study by Roy Chowdhury and colleagues (22), in which the authors have provided a general overview of changes in the main immune blood cells during treatment.

Here, in a prospective, international cohort study of adult patients treated for pulmonary TB in high prevalence countries (Bangladesh and Georgia), peripheral blood T-cell immune-profiles were characterized using a 27-marker mass cytometry panel using samples stimulated with QuantiFERON-TB Gold Plus. In-depth T-cell phenotypical analysis was performed upon TB treatment initiation, after two months and at completion of treatment. To examine the relation between mycobacterial clearance in hosts and changes in T-cell immune-profiles, the results of these analysis were compared in negative and positive sputum culture conversion patients after two months of treatment.

MATERIALS AND METHODS

Experimental Design

Study Design and Research Objectives

This prospective cohort study was nested in a multicentered study coordinated by the Mérieux Foundation GABRIEL network (23). The primary objective was to investigate the association between sputum culture sterilization during TB treatment and T-cell profiles obtained by high-dimensional phenotyping. The sample size was maximized based on availability of clinical samples. No prospective sample size calculations were performed.

Recruitment Centers and Ethical Considerations

Recruitment centers were the National Center for Tuberculosis and Lung Disease (NTCLD) in Tbilisi, Georgia (approval of the Institutional Review Board of the NTCLD; IORG0009467); and the International Centre for Diarrhoeal Disease Research, Bangladesh (icddr,b) in Dhaka, Bangladesh (approval of the Research Review Committee and the Ethical Review Committee of icddr,b; PR-17076; Version No. 1.3; Version date: 04-01-2018). All participants provided written informed consent.

Cohort Recruitment, Patient Follow-up, and Clinical Data Collection

Patients were recruited if diagnosed with sputum culture confirmed pulmonary TB and older than 15 years old. Patients with HIV, immune deficiency, diabetes mellitus, and lost-to-follow-up were excluded. Detailed procedures for microbiological diagnosis, drug susceptibility testing, and treatment regimens are described elsewhere (23). As antimicrobial resistance is a major challenge for TB management and treatment, both drug-susceptible (DS-TB) and drug-resistant (DR-TB) patients were recruited to examine immune profiles in these settings. Patients were followed up: at inclusion (T0), after two months of treatment (T1), and at the end of TB treatment (T2; 6 months for DS-TB patients, 9 to 24 months for DR-TB patients). The T1 timepoint was chosen because it marks the moment after which antibiotic treatment is reduced during clinical DS-TB management. For DR-TB monitoring, the same timepoint was used for consistency. Patients were on Directly Observed Treatment (DOT) and received treatment according to standard protocols (2). Treatment regimens are detailed in **Supplementary Table 1**.

Whole Blood Stimulation and Processing

Detailed whole blood collection and stimulation processes were described elsewhere (24). Briefly, at every follow-up visit, 1mL of whole blood was drawn from the antecubital area of the arm and seeded directly into each QuantiFERON-TB Gold Plus (QFT-P, Qiagen) tube and incubated for 24 hours. Three stimulation conditions were used: NIL as unstimulated control; TB2 which tubes contain a pool of short peptides derived from the *M. tuberculosis* antigensESAT-6 (>15aa) and CFP-10 (8-13aa), optimized to induce responses from $CD4^+$ (25) and $CD8^+$ T lymphocytes (26); and tubes containing recombinant *M. tuberculosis* heparin-binding hemagglutinin generated in *M. smegmatis* at a final concentration of 5µg/mL, named "rmsHBHA" tubes. rmsHBHA antigens were graciously provided by the Delogu laboratory, UNICATT, Rome, Italy (27). After incubation, plasma was separated by decantation and the remaining red fraction was collected and transferred into 15mL

conical tubes. Red blood cell lysis was performed with FACS lysing buffer (BD Biosciences) according to the manufacturer's instructions, and after two washing steps with phosphate buffer saline (PBS), the resulting fixed white blood cells pellets were stored at -80°C. Cryopreserved samples were air-shipped in dry ice with freezing controls to the Mérieux Foundation Emerging Pathogens Laboratory in Lyon, France (International Center for Infectiology Research, INSERM U1111).

Experimental Procedure for Mass Cytometry

Sample Preparation

Cryopreserved cells were thawed and resuspended in PBS to a concentration of $3.5x10^6$cells/mL. Between 1 and $1.5x10^6$ cells from each sample were aliquoted for staining. Cells were incubated 10 minutes with FcR Blocking Reagent (6µL/10^6 cells; Miltenyi Biotec) and heparin sodium salt reconstituted in Millipore water (36µg/10^6 cells; Sigma-Aldrich) to reduce nonspecific staining (28).

Panel Design

A 29-marker panel of metal-labeled antibodies was used. All antibodies were obtained from Fluidigm (**Supplementary Table 2**). Briefly, the panel contained 28 T-cell oriented surface markers (lineage markers, chemokine receptors, activation markers, and exhaustion markers) and one intracellular target (perforin).

Experimental Design and Barcoding

As the study followed a longitudinal design, samples from a same patient were acquired in the same barcoded batch of 3 timepoints and 3 stimulation conditions to reduce experimental variation. Palladium barcoding (29) (Cell-ID 20-Plex, Fluidigm) was performed according to the manufacturer's instructions for simultaneous staining and data acquisition. For each barcoding run, 18 patient T-cell samples were stained with unique combinations of intracellular palladium isotopes (**Figure 1**). Patient batches were processed in a random order and investigators were blinded to patient sputum culture results during data collection.

Staining Procedure

Extracellular staining was performed on pooled barcoded cells in Maxpar Cell Staining Buffer (Fluidigm) for 30 minutes at room temperature. Intracellular staining (perforin) was performed in Maxpar Perm-S Buffer (Fluidigm) for 30 minutes at room temperature. Stained cells were then incubated for 10 minutes in 1.6% formaldehyde (FA) freshly prepared from 16% stock FA (Sigma-Aldrich). DNA staining was performed by overnight incubation at 4°C in 2mL of 125nM Cell-ID Iridium intercalator solution (Fluidigm). Cells were then washed, pelleted, and kept at 4°C until acquisition the same day.

Data Acquisition

Samples were analyzed on a CyTOF2 mass cytometer upgraded to Helios (Fluidigm) hosted by the AniRA cytometry facility (Structure Fédérative de Recherche Lyon Gerland, INSERM U1111, Lyon, France). Samples were filtered twice through a 50µm nylon mesh and resuspended in EQ™ Four Element Calibration Beads (Fluidigm) diluted to 0.5X in Maxpar Cell Acquisition Solution (Fluidigm), to reach an acquisition rate of 150-200 events per second (0.5 x 10^6 cells/mL). Data were collected using the on-board Fluidigm CyTOF software (version 7).

Data Analysis

All data analyses were performed in RStudio (version 1.3.1073 with R version 4.0.3) and FlowJo (version 10.7.1).

Data Cleaning and Preliminary Manual Gating

Signal normalization, concatenation, debarcoding, and conversion into Flow Cytometry Standard (FCS) 3.0 format were performed using the on-board CyTOF Software (Fluidigm). Debarcoded files were imported into FlowJo and arcsinh-transformed. Gaussian parameters of the Helios system were used for doublet exclusion (30, 31), then $^{191}Ir^+$ $^{193}Ir^+$ single events were manually isolated, and debris ($CD45^-$ events) and calibration beads ($^{140}Ce^+$ events) were excluded). A preliminary manual gating analysis was then performed on $CD45^+$ single events (**Supplementary Figure 1**) to check sample quality and verify that the proportions of the main white blood cell subpopulations in biobanked samples were consistent with the expected proportions, and sufficient for downstream analysis. Samples with less than 1,000 $CD3^+$ events were removed in order to reach a sufficient overall event number upon equal down-sampling in downstream analyses. Batches with missing samples from a given timepoint were removed from the analysis to preserve a matched sample design (**Supplementary Figure 2**). The exact number of available files per patient and per stimulation condition is provided in **Supplementary Table 1**. Finally, staining quality was assessed in the samples kept for analysis, in particular for lineage markers and surface markers that were likely to be affected by cell fixation upon collection (e.g. chemokine receptors). Two markers were removed from the initial 29-marker panel, either because signals were undetected (CXCR5), or because non-specific signal was observed (CXCR3).

Workflow for Unsupervised Analyses

$CD3^+$ single events were down-sampled to ensure equal contribution of each sample, exported into separate Comma Separated Value (.csv) files, and uploaded into R software (version 4.0.3). Panel markers were defined as either lineage or functional markers for use as clustering channels in downstream analyses (**Supplementary Table 3**). Lineage-defining markers included canonical surface markers such as CD4 which display a theoretically stable expression. Functional markers included markers of activation (*e.g.* CD69), proliferation (CD38), maturation (CD27), or migration (CCR7).

Dimension Reduction, Automated Clustering, and Phenotyping

After file concatenation, dimension reduction was performed with UMAP (Uniform Manifold Approximation and Projection; version 3.1) (32). UMAPs were created in R using the package Spectre (33). Unsupervised clustering was performed using FlowSOM (34) (version 2.7). FlowSOM meta-cluster phenotyping was assessed by visualizing the surface expression

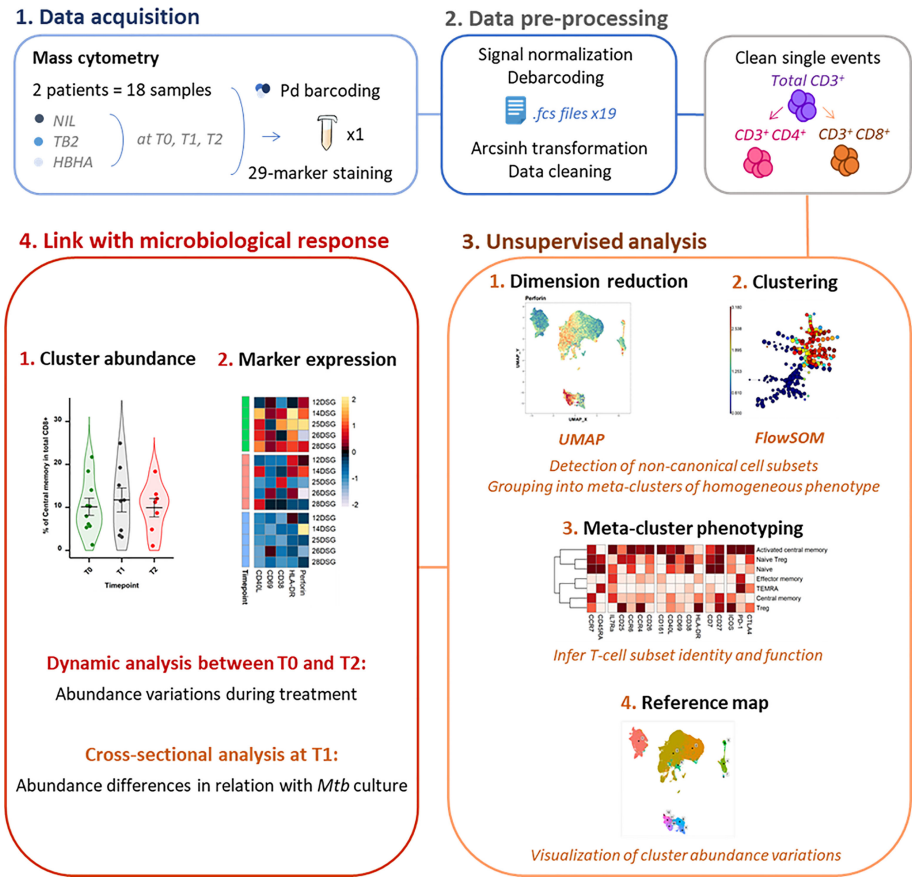

FIGURE 1 | Experimental and analytical workflow. Peripheral whole blood samples were collected from active TB patients (n = 22) throughout treatment (T0: baseline. T1: T0 + 2 months. T2: end of treatment). After whole blood stimulation with *Mtb* antigens (TB2 and rmsHBHA) or with a negative control (NIL), total white blood cells were extracted. After palladium (Pd) barcoding for unique sample identification before multiplexing, T-cells were analyzed with a 29-marker mass cytometry panel. TB2, Qiagen QuantiFERON TB2 tube (ESAT-6 + CFP-10 + undisclosed $CD8^+$ T-cell stimulating peptide pool); rmsHBHA, recombinant heparin-binding hemagglutinin obtained in *Mycobacterium smegmatis*; UMAP, Uniform Manifold Approximation and Projection; FlowSOM, self-organizing map.

of lineage markers in each FlowSOM cluster (CD4, CD8, TCRgd, TCRVa7.2, CD56, CD25, IL7Ra, CD26, and CD161) on a heatmap and performing hierarchical clustering. Marker expression heatmaps were obtained in R using Spectre by plotting normalized, median arcsinh-transformed mass signals. Biological consistency of FlowSOM meta-clusters with the main expected T-cell subpopulations was controlled (**Supplementary Figure 3** and **Supplementary Table 3**). Meta-clusters with an abundance <1% of all events were pooled with the most phenotypically similar meta-cluster. Then, the proportion of corrected FlowSOM meta-clusters in each node on the initial FlowSOM minimum spanning tree was visualized to control reassignment consistency (35).

Statistical Analysis

The proportion (percent of $CD3^+$) of each FlowSOM cluster was calculated. For all statistical analyses, exact p-values, test statistics and/or estimates of effect size are provided either in the figure legend or in indicated **Supplementary Tables**. Normality was assessed using the Shapiro-Wilk test. The evolution of cluster proportions over time corresponded to repeated measures of non-normal, non-independent continuous variables, and was analyzed in matched samples using the two-sided Friedman rank sum test with the Wilcoxon–Nemenyi–McDonald-Thompson *post-hoc* test (36). Independent, non-normal continuous variables were analyzed with the two-sided Mann–Whitney U test. For discovery of clusters with significantly different abundance between slow and fast converters, conservative corrections for multiple comparisons [e.g. Benjamini-Hochberg (37)] were performed as an indication and are presented as **Supplementary Data**, but were not used for cluster discovery in order to minimize type II errors as they were too conservative for this small, exploratory pilot study (38). For cluster selection for phenotype analysis, all p-values were computed for each timepoint, and the p-value corresponding to the null hypothesis being rejected in 5% of all comparisons was used as the significance threshold instead of 0.05 (38). This novel significance threshold enabled to reduce the frequency of false discovery while maintaining an exploratory approach; its value was always inferior to 0.05 and is reported in the corresponding figure captions.

RESULTS

Study Design and Analysis Strategy

Between May 2019 and July 2020, 144 cell samples collected from 22 adult TB patients were analyzed (Bangladesh, n=4 and Georgia, n=18; DS- and DR-TB, n=11 each) (**Supplementary Figure 2**). Patient demographic, microbiological and clinical characteristics are available in **Supplementary Table 1**. All patients achieved microbiological cure at the end of treatment, but were retrospectively classified into two response groups according to their *M. tuberculosis* culture status at T1 (after two months of treatment): fast converters (n=18; negative culture at T1 and T2) and slow converters (n=4; positive culture at T1 and negative culture at T2). Among the latter, three patients were treated for DS-TB and one for DR-TB.

Overall Analysis of Peripheral T Lymphocyte Subset Abundance Changes Throughout TB Treatment

First, a phenotype analysis was performed to identify the main expected T-cell subpopulations. As no apparent difference was seen in UMAP structures within samples from the different timepoints and stimulation conditions despite some marker expression differences between stimulation conditions (**Supplementary Figure 4**; exact p-values and test statistics in **Supplementary Table 4**), we performed the phenotype analysis on all single $CD3^+$ events. The purpose of this study was not to compare the stimulations, but rather to use them to uncover clusters that might be associated with treatment response and that would not be visible in unstimulated samples. FlowSOM automated clustering was performed on $CD3^+$ events, revealing a total of 196 automatically detected clusters (**Figures 2A–C**). They were automatically grouped into 18 meta-clusters, which were assembled into 12 canonical T-cell subpopulations in a supervised manner (**Figures 2D, E**). FlowSOM clusters and meta-clusters were then visualized on the initial UMAP to create a reference map of all automatically detected T-cell subsets (**Figures 2F, G**).

To initiate the abundance analysis, variations of the main T-cell subpopulations throughout treatment were then studied using a stratification according to each stimulation condition. No significant change in the proportion of total $CD4^+$, $CD8^+$, γδ, double negative (DN, $CD4^-$ $CD8^-$) or double positive (DP, $CD4^+$ $CD8^+$) T-cells was observed throughout treatment in any stimulation condition (**Supplementary Figure 5**). For all main studied subpopulations, no significant difference was observed between DS- and DR-TB patients (data not shown).

Differential Abundance of Non-Canonical T-Cell Subsets Throughout TB Treatment

To identify non-canonical T-cell subsets whose abundance changed throughout treatment, we calculated the percentage of each automatically determined FlowSOM cluster at each timepoint and in each stimulation condition. These clusters were then categorized into two groups: enriched or decreased after treatment completion. Abundance changes were studied between T0 and T1 and T0 and T2 to characterize the main clusters associated with response to treatment intensive phase and with treatment completion respectively. As these clusters represent non-canonical cell subpopulations, their frequencies among total $CD3^+$ events were low (< 5% in most samples). Hence, the differences analyzed thereafter describe rare populations and warrant cautious analysis.

When comparing the reference UMAP (**Figure 2G**) to the UMAP of clusters which were increased between T0 and T1 (**Supplementary Figure 6A**), we observed that they were either DN T-cells, or effector memory (EM) or terminally differentiated effectors re-expressing CD45RA (TEMRA) cells from both $CD4^+$ and $CD8^+$ subpopulations. In unstimulated samples, significant increases were detected within three clusters corresponding to $CD8^+$ and DN T-cell subsets, whereas increases were detected in one $CD4^+$ and one $CD8^+$ cluster in TB2-stimulated samples, and only in $CD4^+$ clusters in rmsHBHA samples (**Supplementary Figure 6B**); Clusters that decreased between T0 and T1 (**Supplementary Figure 6C**) were detected only within $CD8^+$ EM and TEMRA cells in all stimulation conditions (**Supplementary Figure 6D**).

Between T0 and T2, 11 increased clusters were detected (**Figure 3A**). They corresponded mostly (8/11 clusters, 73%) to $CD4^+$ EM and CM subpopulations rather than naïve subsets, regardless of the stimulation condition (**Figures 3B–D**). One DN cluster was increased in unstimulated samples (**Figure 3B**) as well as one $CD8^+$ TEMRA cluster and one γδ T-cell cluster in rmsHBHA stimulated samples (**Figure 3D**). One $CD4^+$ CM cluster (number 38) increased significantly in samples from all three stimulation conditions. Clusters which decreased between T0 and T2 were detected in one $CD8^+$ EM and two $CD8^+$ TEMRA subsets, and in seven clusters within $CD4^+$ subpopulations in all three stimulation conditions (**Figures 3E–H**). Regarding the latter clusters, no clear trend was observed regarding memory subset compartmentalization, which suggests that the abundance decrease spared memory functions and rather affected $CD4^+$ T-cells in general. One γδ and one DN T-cell cluster also decreased significantly within *Mtb*-stimulated samples (**Figures 3G, H**).

Cluster Abundance Changes During TB Treatment Show Involvement of Effector and Memory T-Cells

To further refine patterns in functional marker expressions within increased or decreased clusters, we then performed a detailed phenotype analysis using marker expression heatmaps and hierarchical clustering (**Figure 4**). Four subgroups of cellular subsets of similar abundance changes and similar immunophenotypes were identified (labeled from A to D). Subgroup A included three $CD8^+$ T-cell clusters that decreased throughout treatment between T0 and T2. Consistently with the above results (**Figure 3E**), the latter were either EM or TEMRA cells, with low CD45RA levels and intermediate levels of perforin. Subgroup A included four $CD4^+$ T-cell clusters with naive (n=2) and CM (n=2) phenotypes, which decreased from T0 to T2 in rmsHBHA-stimulated samples.

In contrast, subgroup C and D included only $CD4^+$ T-cell clusters which increased between T0 and T2. Subgroup C clusters had an EM phenotype (clusters 28 and 54) or a CM phenotype with low levels of CCR7 (clusters 38 and 69). Subgroup D consisted in

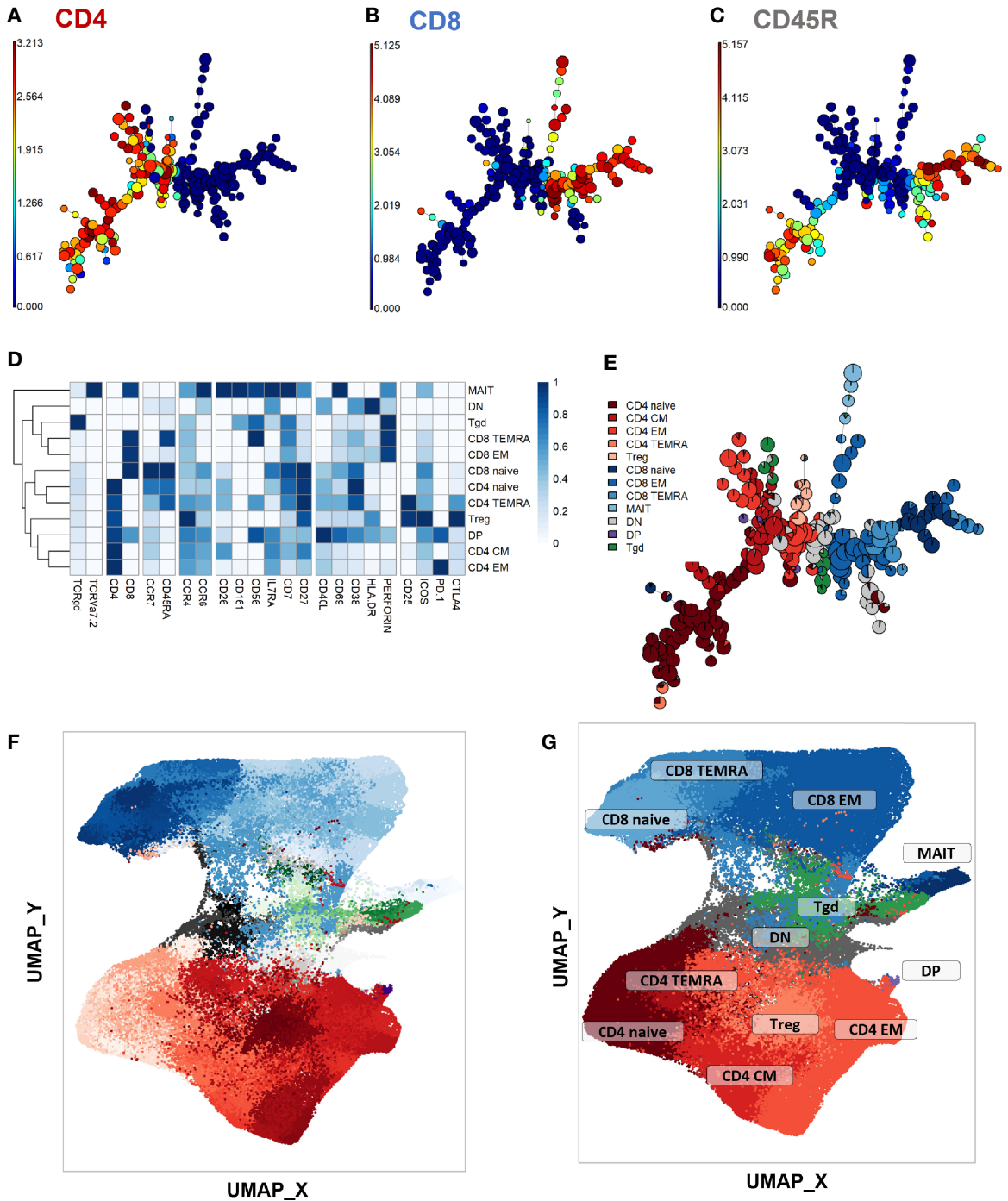

FIGURE 2 | Peripheral CD3$^+$ T-cell unsupervised clustering and phenotyping. **(A–E)** FlowSOM automated clustering. The surface expression of lineage markers used for FlowSOM calculations was visualized in all CD3$^+$ events (201,000 events from equally down-sampled files) regardless of timepoint or stimulation. FlowSOM enabled automated repartition of CD3$^+$ events into 196 clusters according to the surface expression of selected lineage markers such as CD4 **(A)**, CD8 **(B)**, and CD45RA **(C)**. Scales indicate arcsinh-transformed mass signal values. Clusters were automatically grouped into 18 meta-clusters of homogeneous phenotype, which were assembled into 12 canonical T-cell subpopulations in a supervised manner after meta-cluster phenotyping. This was performed with heatmap visualization of normalized, arcsinh-transformed median mass signal values for each surface marker **(D)**. The proportions of the resulting T-cell subpopulations were visualized on the initial FlowSOM minimum spanning tree to control phenotyping consistency **(E)**. **(F, G)** Reference mapping. Dimension reduction was performed with UMAP and overlayed with automatically determined FlowSOM clusters **(F)** and meta-clusters **(G)** to generate a phenotype reference map. Cluster labels were not displayed for legibility. CM, central memory; DN, double-negative CD4$^-$CD8$^-$; DN, double-positive CD4$^+$ CD8$^+$; EM, effector memory; MAIT, mucosal associated invariant T-cells; Tgd, gamma delta T-cells; Treg, T-regulators; TEMRA, terminally differentiated effectors re-expressing CD45RA.

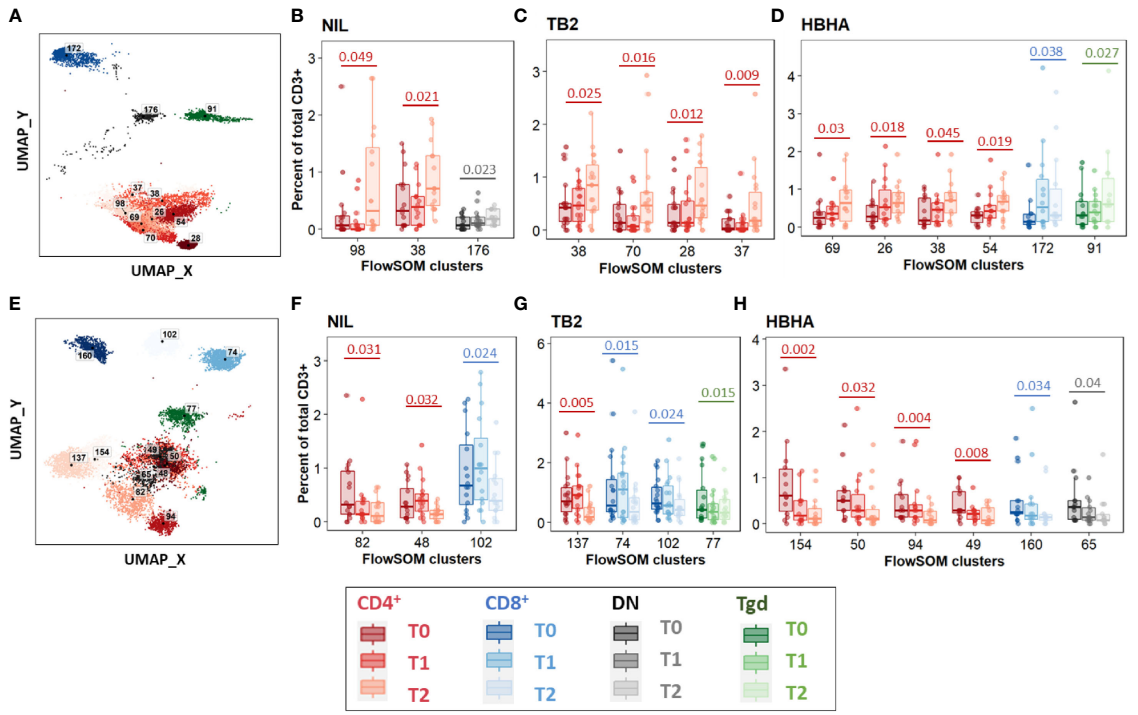

FIGURE 3 | Significant abundance changes in non-canonical T-cell subsets throughout TB treatment. FlowSOM cluster abundance was analyzed over time in unstimulated or *Mtb*-stimulated samples (TB2 or rmsHBHA). Only clusters within which significant abundance changes were detected were displayed. Number of matched data points per timepoint for all panels: NIL: n = 16. TB2: n = 18. rmsHBHA: n = 14. Data are represented as medians + interquartile range. **(A–D)**. Significantly increased clusters at treatment completion (T2) compared to treatment initiation (T0). Clusters within which a significant increase was detected between T0 and T2 were visualized on the reference UMAP shown in **Figure 3 (A)**. Cluster abundance quantification was was performed in unstimulated **(B)**, TB2-stimulated **(C)** or rmsHBHA-stimulated samples **(D)**. **(E–H)** Significantly decreased clusters at treatment completion (T2) compared to treatment initiation (T0). Mapping **(E)** and abundance quantification of clusters which increased between T0 and T2 in unstimulated **(F)**, TB2-stimulated **(G)** or rmsHBHA-stimulated samples **(H)**. DN, double negative $CD4^-$ $CD8^-$; Tgd, gamma delta T-cells. Statistical analysis: Friedman rank sum test and Wilcoxon-Nemenyi-Thompson *post-hoc* for pairwise comparisons between non-independent observations at T0, T1, and T2. Exact, unadjusted p-values are indicated on the figures. Benjamini-Hochberg corrections for multiple comparisons were performed as an indication and were not used for cluster selection for phenotype analyses in order to minimize type II errors. Adjusted p-values did not reach significance. All adjusted p-values and complete test statistics are available in **Supplementary Table 5**.

three clusters exhibiting an CM phenotype and expressing activation markers, detected in unstimulated and TB2-stimulated samples. Clusters from these two subgroups co-expressed CD26, IL7Ra, CD7 and CD27. They were characterized by an absence of activation marker expression and an enhanced expression of exhaustion markers, in particular CTLA-4 and PD-1. Overall, we observed T-cell subset abundance changes between T0 and T2. In TB2 and rmsHBHA samples, $CD4^+$ EM clusters mostly increased, while $CD8^+$ EM clusters mostly decreased.

Individual Profiling Confirms Abundance Changes in Phenotypically Homogeneous, Correlated Subsets After Treatment in Cured Patients

As the differentially abundant clusters identified above accounted for a small fraction of $CD3^+$ T-cells (<1%), we intended to identify the largest possible subsets of phenotypically homogeneous cells within which a significant abundance change was detectable (**Figure 5**). Within the subgroups of similar immunophenotypes and abundance change identified in **Figures 3**, **4**, we performed correlation analyses on the cluster abundance at baseline and pooled the best correlated clusters together within the subgroups identified in **Figure 4** (**Figures 5A, D**). We then visualized the individual abundance change of these pooled subsets before and after treatment completion in cured patients (**Figures 5B, C, E, F**). Within unstiumlatedsamples, a decrease in subgroup A and an increase in subgroup D were both detected in 83% (13/16) of cured participants (**Table 1**). Within rmsHBHA stimulated samples, a decrease in subgroup B and an increase in subgroup C were recorded in 93% (13/14) of patients. This confirmed that the median trends observed previously were maintained individually in most patients.

Finally, we visualized the immunophenotypes of these four subgroups of interest in comparison to cells from similar subpopulations which were not associated to cure (**Figure 5G**). Subgroup A corresponded to $CD8^+$ $CD7^+$ $Perforin^+$ EM cells. Subgroup B corresponded to $CD4^+$ naive cells expressing high levels of CD26, as well as CCR6, IL7Ra, CD7, CD27, HLA-DR, and CD38. Subgroup C and subgroup D respectively

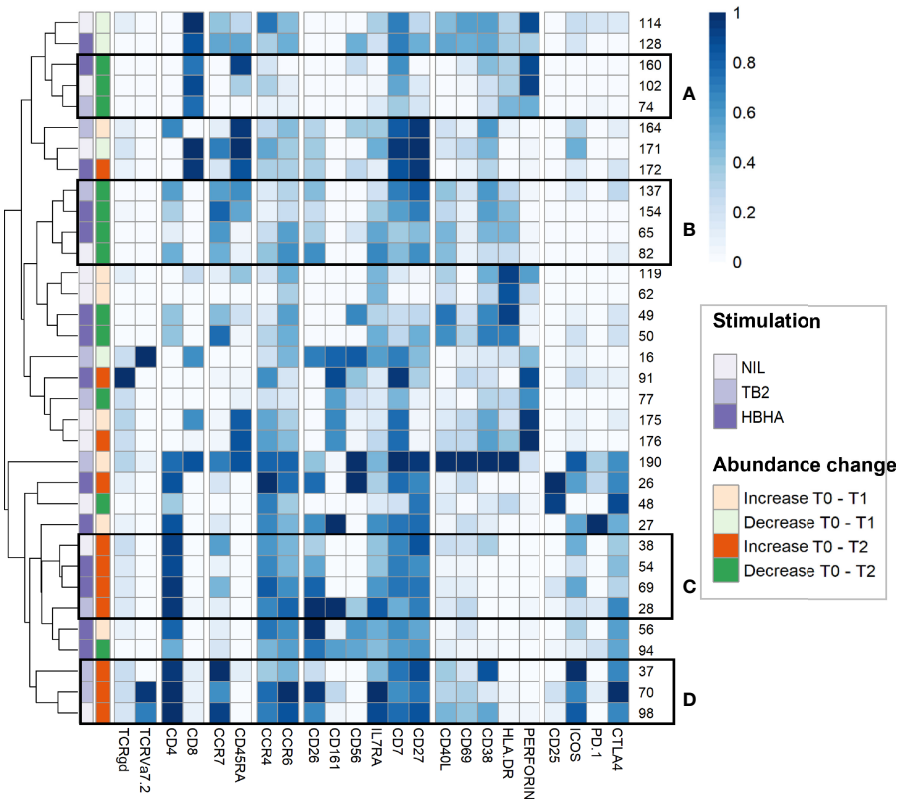

FIGURE 4 | In-depth phenotyping shows differential involvement of effector and memory T-cells in cluster abundance changes during TB treatment. Mean marker expression levels were visualized using heatmapping for cell cluster which increased (orange color code) or decreased (green color code) throughout treatment. Each line represents one cell cluster. Scales indicate normalized mass signal intensity. Hierarchical clustering was performed based on marker expression levels, regrouping cell clusters of similar immunophenotypes. Black rectangles annotated from **(A–D)** indicate cell cluster subgroups with both similar abundance changes and similar immunophenotypes (i.e. at least same main T-cell subset).

corresponded to $CD4^+$ EM or CM cells expressing CCR4, CCR6, IL7Ra, CD27, and CD38. Cells within subgroup C expressed high levels of CD26 and CD7 than other CD4+ EM cells. Finally, we verified these findings by manually gating the identified subpopulations and comparing the percentages at T0 and T2 (**Figures 5G–K**, representative dot plots).

Patients With Persistent Positive Cultures at T1 Show Decreased Peripheral $CD8^+$ Cytotoxic Subsets and Enriched Peripheral $CD4^+$ Naïve Subsets Throughout Treatment Compared to Patients With Negative Cultures at T1

Then, we aimed to detect a cellular signature associated with mycobacterial conversion. To do so, we analyzed individual cluster abundance in slow vs. fast converters throughout treatment. At T0, T1, and T2, respectively 21, 24, and 21 clusters with significantly different abundance in slow converters compared to fast converters were detected (quantification in **Supplementary Figure 6**). After phenotyping, the proportions of the main T-cell subpopulation phenotypes in each group of enriched or decreased clusters at T0, T1, and T2 were calculated and summarized in **Table 2**. As a validation step, manual gating of cell subpopulations representative of the main cluster subsets identified was performed and compared between fast and slow converters (an example at T1 was shown in **Supplementary Figure 9**).

Before treatment initiation, of 21 clusters with different abundance, 18 (86%) were decreased (**Supplementary Figure 7A**) and three (14%) were enriched (**Supplementary Figure 7B**) in slow compared to fast converters. Clusters which were under-represented in slow converters corresponded mostly to DN, γδ, and $CD8^+$ T-cells (77%, 13/18 clusters), specifically γδ and $CD8^+$ EM T-cell subpopulations (38%, 5/13 each); in addition, a majority of these clusters was $perforin^+$ (67%, 12/18) (**Supplementary Figure 8A**). In contrast, the three enriched clusters were naive $CD4^+$ and $CD8^+$ T-cells, as well as one $CD8^+$ TEMRA subset.

At T1, of 24 clusters with significantly different abundance between slow and fast converters, 15 (62%) were decreased (**Figures 6A, C**) and 9 (38%) were enriched in slow converters (**Figures 6B, D**). These clusters were mostly detected in TB2-stimulated samples (63%; 15/24 clusters). Comparison to the reference UMAP (**Figure 6E**) and hierarchical clustering

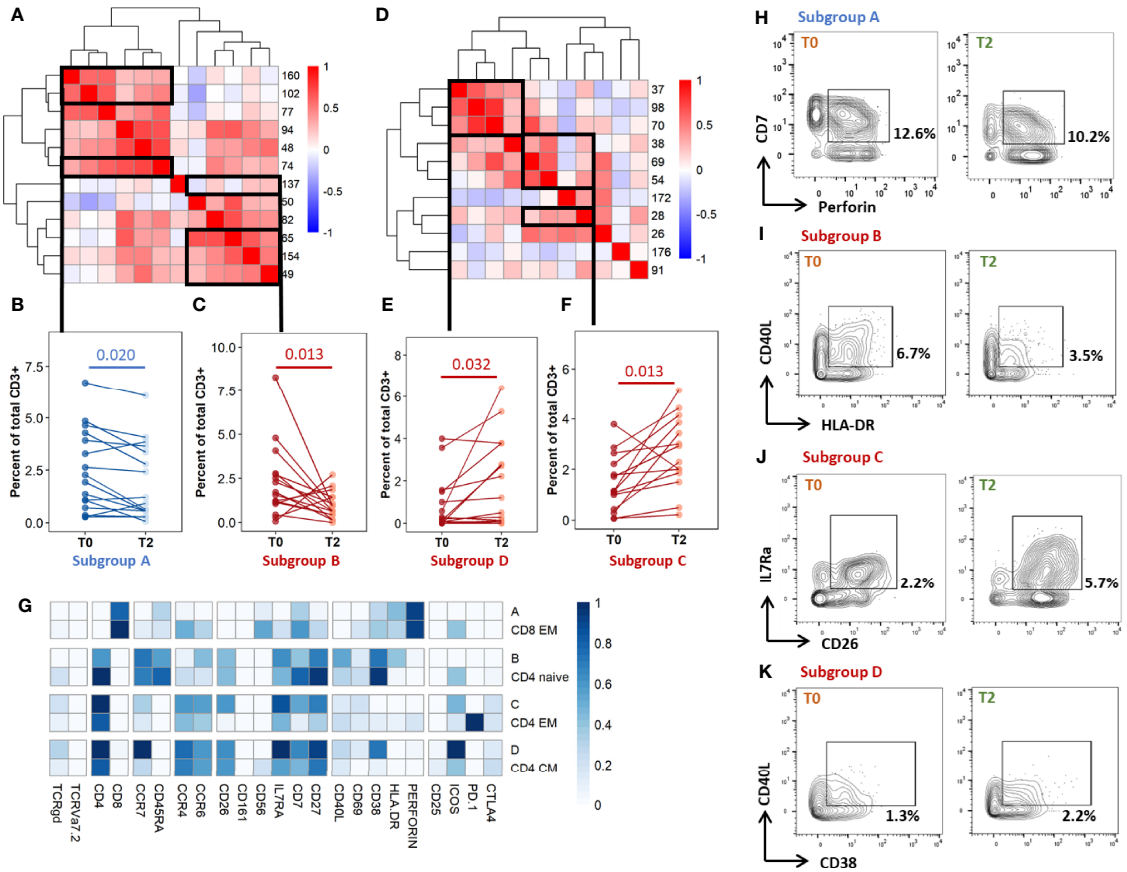

FIGURE 5 | Individual immunoprofiling confirms differential abundance of correlated subsets in cured patients after treatment. Cluster were stratified by type of significant abundance change: enrichment **(A-C)** or depletion **(D-F)** after treatment completion. **(A, D)** Pearson's correlations were calculated on cluster abundance at T0 and displayed on a heatmap with hierarchical clustering. Clusters with similar immunophenotypes (**Figures 3**, **4**) and positive correlation coefficients were grouped. Estimates of effect sizes are in **Supplementary Tables 6, 7**. **(B, C, E, F)** The abundance of each subgroup was visualized. Each dot represents data for one patient. Statistical analysis: Friedman rank sum test. Subgroup A: data from rmsHBHA samples (n =14), clusters 74, 102, 160; p = 0.020, Fchisq = 5.4. Subgroup B: data from unstimulated samples (n =16), clusters 137, 154, 65, 82; p = 0.0013, Fchisq =10.3. Subgroup C: data from unstimulated samples, clusters 38, 54, 69, 28; p = = 0.0013, Fchisq = 10.2. Subgroup D: data from rmsHBHA samples, clusters 37, 70, 98; p = 0.032, Fchisq = 4.57. **(F)** For each subgroup, normalized mean marker expression levels were compared with similar T-cell subsets. **(G–K)** Manual gating analysis was performed to verify unsupervised results (representative plots, 500 to 1,000 events). Numbers indicate the percentage of gated cells among total $CD3^+$ cells. Subgroup A: $CD3^+CD8^+CCR7^-CD45RA^-CD7^+Perforin^+$. Subgroup B: $CD3^+$ $CD4^+CCR7^+CD45RA^-CCR6^+IL7Ra^+CD27^+CD40L^+CD38^+HLA\text{-}DR^+$. Subgroup C: $CD4^+CCR7^{low}CD45RA^-CCR4^+CCR6^+$ $CD26^+IL7Ra^+CD7^+CD27^+$. Subgroup D: $CD4^+CCR7^+CD45RA^-CCR4^+CCR6^+CD26^+IL7Ra^+CD7+CD27^+$ $CD38^+$.

(**Figure 6F**) indicated that enriched and decreased subsets respectively had similar immunophenotypes. Clusters which were under-represented at T1 in slow converters were mostly $perforin^+$ cells (67%, 10/15 clusters); mostly $CD8^+$ TEMRA and DN T-cell phenotypes were represented (40%, 6/15 clusters respectively). In contrast, enriched clusters comprised a majority of $CD4^+$ T-cells (78%, 7/9 clusters), with predominantly naïve phenotypes (45%, 3/7). One $CD8^+$ naive and one $CD8^+$ EM cluster were also enriched in slow converters at T1, with the latter expressing ICOS.

After treatment completion, of 21 clusters with significantly different abundance between slow and fast converters, 11 (52%) were decreased (**Supplementary Figure 7C**) and 10 (48%) were enriched in slow converters (**Supplementary Figure 7D**). The immunophenotype profile at T2 was similar to that of T1 for the enriched subsets: a majority of $ICOS^+$ $CD4^+$ naïve T-cell subsets (50%, 5/10) were detected, as well as two $CD8^+$ naïve clusters (**Supplementary Figure 8B**). Regarding the decreased subsets, no specific phenotype polarization was observed, and clusters were detected within diverse subsets (four $CD8^+$ EM clusters, four $CD4^+$ EM clusters, and three DN T-cells clusters). Similarly to the T1 immune profile, all of the above clusters were mostly detected in TB2-stimulated samples (67%, 14/21 clusters).

Maturation Markers and Chemokine Receptors, Rather Than Activation or Cytotoxic Markers, Discriminate Slow From Fast Converters During Treatment

Finally, we sought to assess more precisely which combinations of cellular markers were the most involved in the

TABLE 1 | Selected subset abundance changes before and after treatment completion.

Sample	Abundance between T0 and T2 (%, N)
Subset A decreased	
NIL (n=16)	**81% (13)**
TB2 (n=18)	72% (13)
rmsHBHA (n=14)	71% (10)
Subset B decreased	
NIL	75% (12)
TB2	83% (15)
rmsHBHA	**93% (13)**
Subset C increased	
NIL	69% (11)
TB2	83% (15)
rmsHBHA	**93% (13)**
Subset D increased	
NIL	**81% (13)**
TB2	72% (13)
rmsHBHA	57% (8)

*These data were obtained from **Figure 5**.*
Bold values represent the stimulation condition in which the highest percentage of abundance changes of the same type (increase or decrease) were detected.

discrimination between fast and slow converters within the clusters identified in the prior section. A principal component analysis (PCA) was performed on marker expression data within these clusters. As a higher number of differentially abundant clusters had been detected in *Mtb*-stimulated samples than in unstimulated samples during treatment (T1 and T2), and because a complete overlap between the PCA profiles of fast and slow converters was observed in unstimulated samples, we focused on *Mtb*-stimulated samples (TB2 and rmsHBHA). PCA profiles were mostly separated when split by culture conversion group (**Figure 7A**). Dimension 1 (Dim1) explained 38.2% of the total observed variance, versus 12.6% for Dim2. The main markers accounting for variance described by Dim1 were markers of memory subset definition (CCR7 and CD45RA), lineage (CD4 and TCRγδ), maturation (CD27 and CD7), chemokine receptors (CCR4) or other receptors or costimulatory molecules (e.g., CD26, CD161) (**Figures 7B, C**). In contrast, variance described by Dim2 was mostly explained by cytotoxicity (Perforin, CD56, CD8), activation (CD38, CD40L, CD69), or exhaustion markers (CD152, PD-1) (**Figures 7B, D**). The PCA scores were significantly higher in slow converters than in fast converters at all timepoints for Dim1 (**Figure 7E**), indicating that the immune profile of slow converters was more correlated to Dim1 than that of fast converters regardless of the timepoint. In contrast, no significant differences were detected at the end of treatment (T2) for Dim2 (**Figure 7F**).

DISCUSSION

In a population of adults treated for TB, we observed a shift towards more differentiated profiles among peripheral $CD8^+$ and $CD4^+$ T-cell subsets driven by the timing of *Mtb* culture conversion, using a high-dimensional single cell approach after stimulation with standardized, IVD-level TB2 antigens. In particular, differentiated $CD8^+$ cytotoxic effector subsets were under-represented in positive- versus negative-sputum culture patients after two months of treatment.

Over the course of TB treatment, we observed as a general trend that cellular subsets within CM $CD4^+$ and TEMRA $CD8^+$ populations increased, whereas naïve $CD4^+$ and naïve/EM $CD8^+$ subsets decreased. This trend is consistent with prior works addressing T-cell differentiation and T-cell memory subsets during TB treatment (39–41). *Mtb*-specific $CD4^+$ EM T-cells have been associated with active TB disease, whereas CM T-cells have been associated to latency and increased upon treatment (42, 43). In *Mtb*-specific $CD8^+$ T-cells, an overall decrease in peripheral blood (44) and a decrease in CM cells (45) have been documented after treatment. In contrast, the central result of this study was to distinguish negative- from positive-sputum culture patients at two months, whether infected with a DS- or DR-*Mtb* strain, through differential peripheral T-cell populations. When retrospectively analyzing the T-cell profiles of fast and slow converters at diagnosis, a pre-existing difference in percentages

TABLE 2 | Proportions of the main T-cell subpopulations within enriched or decreased subsets in slow converters compared to fast converters.

Abundance in slow vs. fast converters	T0 (21 clusters)		T1 (24 clusters)		T2 (21 clusters)	
	Decreased	Enriched	Decreased	Enriched	Decreased	Enriched
	86% (18)	**14% (3)**	**62% (15)**	**38% (9)**	**52% (11)**	**48% (10)**
Total $CD8^+$ and γδ	72% (13)	67% (2)	53% (8)	22% (2)	36% (4)	20% (2)
γδ T-cells	38 (5)	–	–	–	–	–
$CD8^+$ TEMRA	24 (3)	50 (1)	75 (6)	–	–	–
$CD8^+$ EM	38 (5)	–	25 (2)	50 (1)	100 (4)	–
$CD8^+$ naïve	–	50 (1)	–	50 (1)	–	100 (2)
Total $CD4^+$	11% (2)	33% (1)	7% (1)	78% (7)	36% (4)	80% (8)
$CD4^+$ EM	50 (1)	–	100 (1)	29 (2)	100 (4)	–
$CD4^+$ CM	50 (1)	–	–	14 (1)	–	38 (3)
$CD4^+$ naïve	–	100 (1)	–	43 (3)	–	62 (5)
Total DN	17% (3)	0	40% (6)	0	27% (3)	0

*These data were obtained from **Figure 6** and **Supplementary Figure 6**. Data are given as percentage of clusters in each category (number of clusters in each category/total number of decreased or enriched clusters).*

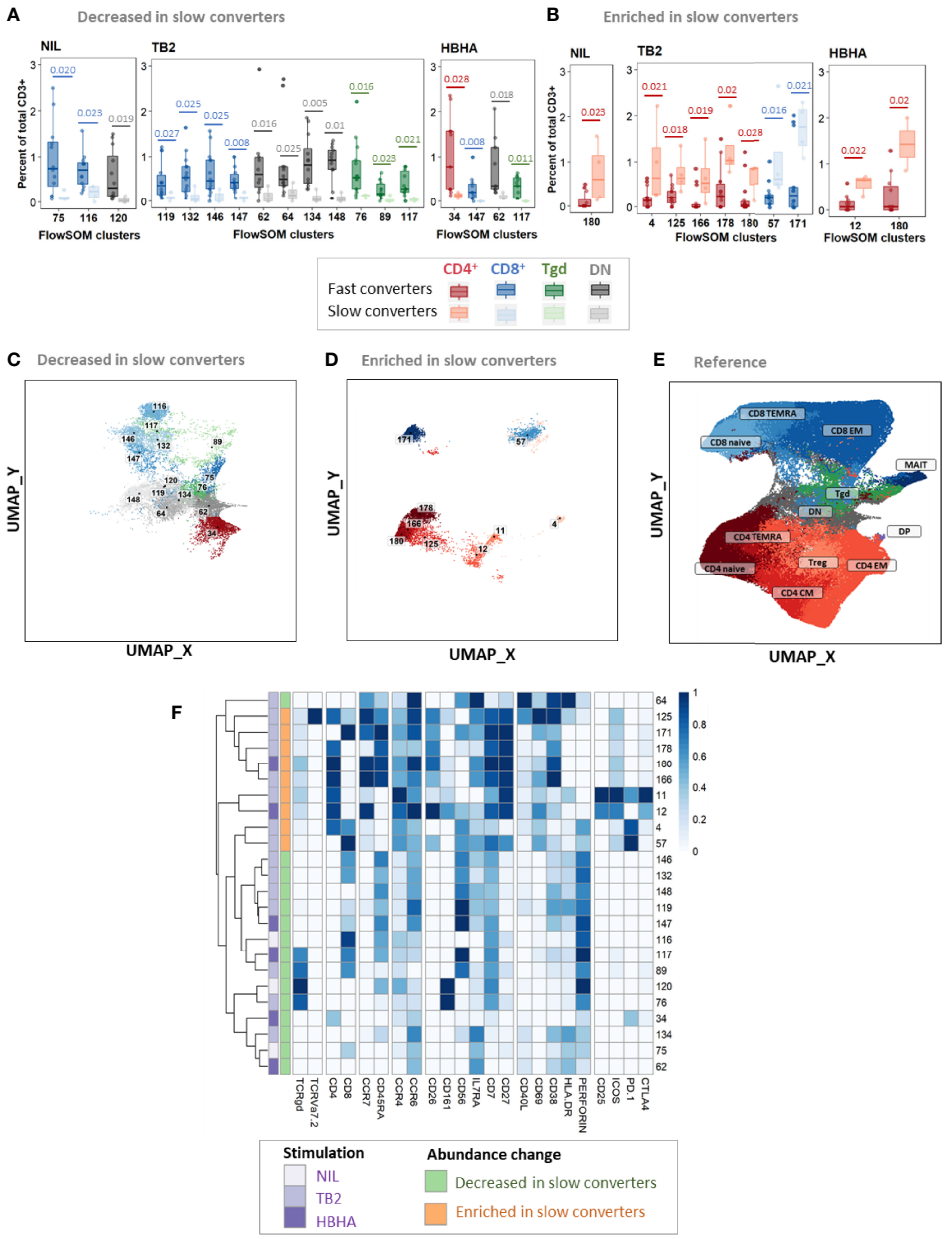

FIGURE 6 | Patients with slow microbiological culture conversion show decreased cytotoxic CD8$^+$ and γδ enriched CD4$^+$ naïve T-cell subsets before treatment initiation and after two months of treatment compared to fast converters. Fast converters (n = 18) were defined as patients with permanently negative *M. tuberculosis* culture after two months of treatment (T1), whereas slow converters (n = 4) were defined as patients with persistently positive cultures at T1. The abundance of all FlowSOM clusters at baseline was compared between fast and slow converters. CD4$^+$ clusters were represented in red, CD8$^+$ clusters in blue, and γδ T-cell clusters in green. Clusters which were significantly decreased **(A, C)** or enriched **(B, D)** at T1 in slow converters compared to fast converters were compared to the reference UMAP **(E)**. Normalized, arcsinh-transformed mean marker expression levels were visualized **(F)**. Each row represents one cluster. Scales indicate normalized mass signal intensity. Boxplot data represent medians + interquartile range. Statistical analysis: Only clusters within which differences passing a threshold of p<0.035 (Mann-Whitney U test) were represented. Exact, unadjusted p-values are indicated on the figures. Benjamini-Hochberg corrections for multiple comparisons were performed as an indication and were not used for cluster selection for phenotype analyses. Adjusted p-values did not reach significance. All adjusted p-values and complete test statistics are available in **Supplementary Table 8**.

of cytotoxic EM CD8$^+$ T-cell subpopulations was already observed. After two months of treatment, this trend shifted into an under-representation of CD8$^+$ TEMRA, which persisted after cure. These changes were revealed upon stimulation with QFT-P TB2 antigenic peptide pools. Although many studies characterizing T-cell subsets during treatment have clearly underlined the importance of *Mtb*-specific CD4$^+$ T-cells (9, 13, 46), less is known about the role of CD8$^+$ T-cells in TB

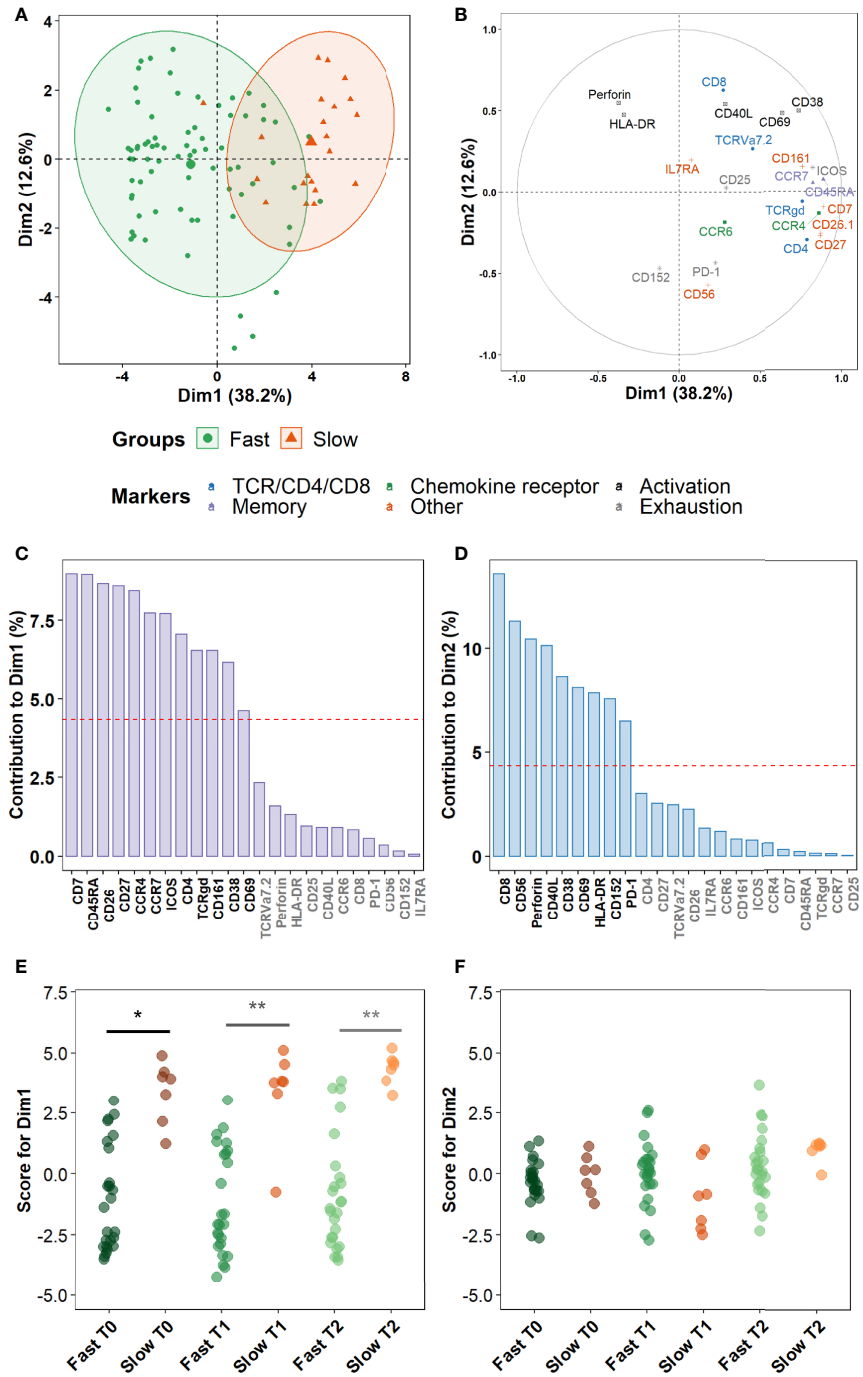

FIGURE 7 | Non-lineage markers discriminate slow and fast responders within differentially abundant subsets. Principal Component Analysis (PCA) was performed on marker expression data from the clusters identified in **Figure 6**, within 96 *Mtb*-stimulated samples matched at T0, T1, and T2 (TB2: 54 samples; rmsHBHA: 42 samples; see **Supplementary Table 1** for sample number details). **(A)** Explanation of the variance between fast converters (25 samples at each timepoint) and slow converters (7 samples at each timepoint). Axes represent the principal components 1 (Dimension 1, Dim1) and 2 (Dim2). Percentages indicate their contribution to the total observed variance. Axis values represent individual PCA scores. Concentration ellipses correspond to 90% data coverage. **(B)** Contribution of cellular markers to the variance described by Dim1 and Dim2. Axis values represent marker PCA scores. Color codes represent broad marker functions. **(C, D)** Quantification of **(B)** for Dim1 **(C)** and Dim2 **(D)**. Contributions of each marker are expressed as a percentage of the dimensions. The dashed line corresponds to the expected reference value if each marker contributed uniformly to the variance. Markers indicated in gray are below this reference value. **(E, F)** Distribution of individual PCA score values according to the culture conversion group at each timepoint, for Dim1 **(E)** and Dim2 **(F)**. Wilcoxon Rank Sum Test. *$p < 0.05$. **$p < 0.001$. Exact p-values and test statistics are in **Supplementary Table 9**.

resolution and the most appropriate epitopes to study them in this context (47, 48). Yet, effector $CD8^+$ T-cells are known to secrete cytolytic and antimicrobial factors that kill *Mtb*-infected macrophages *in vitro* (49), inhibit *Mtb* growth (47), and are required for long-term infection control in mice (50) and humans (51); perforin production by $CD8^+$ T-cells is also higher in treated than in untreated TB patients (52). In addition, a 2012 study by Rozot and colleagues had associated *Mtb*-specific TEMRA $CD8^+$ T cells to LTBI and EM cells to active TB (53). Here, although we cannot establish causality, a lower peripheral $CD8^+$ TEMRA subset abundance may be associated with slower mycobacterial culture conversion. In relation with abundance changes during treatment, our study hints that the $CD8^+$ T-cell phenotype shift occurring during TB treatment would be delayed in patients with slower microbiological conversion. Consistently, it has been shown that $CD8^+$ response importantly contributed to the control of other granulomatous infections such as *Brucella* (54). Regarding $CD4^+$ T-cells, naïve subsets were over-represented in slow converters, which suggests a delayed differentiation within the $CD4^+$ compartment as well. Previous work has shown that the IFN-γ/IL-2/TNF-α functional profile of *Mtb*-specific $CD4^+$ T-cells, which is key in anti-TB immunity (17), was correlated with their degree of differentiation (55). Taken together, these results support the hypothesis that $CD4^+$ and $CD8^+$ T-cell responses should be monitored together during TB treatment, as successful mycobacterial clearance involves $CD8^+$ T-cell effectors, which in turn require $CD4^+$ T-cell involvement (56). In addition, our study also identified some DN cell subpopulations which were relevant for treatment monitoring. We hypothesized that some of these DN clusters may encompass γδ T-cells which could not be identified using out TCRgd clone, as well as $TCRVa7.2^+$ DN MAIT cells. This would be consistent with the cytotoxic phenotypes that these clusters exhibited, and warrants further investigation.

Our study highlights differential *Mtb*-specific $CD8^+$ T-cells marker profiles according to the nature of the antigen stimulation, consistently with previous work (57). We used QFT-P TB2, which elicits cytotoxic $CD8^+$ responses in addition to ESAT-6/CFP-10-induced $CD4^+$ responses (25), as well as rmsHBHA, a recombinant *Mtb* protein exposing many different epitopes. The latter was included because the IFN-γ response to HBHA, to which both $CD4^+$ and $CD8^+$ cells participate (58), is impaired in active TB patients and restored during treatment (24, 59, 60). Here, changes during treatment in $CD8^+$, $CD4^+$, DN, and γδ T-cell subsets were detectable within unstimulated and TB2 samples, consistently with previous works (25). In contrast, in rmsHBHA-stimulated samples, significant abundance changes were mostly detected within $CD4^+$ T-cells, suggesting a preferential $CD4^+$ T-cell response to HBHA epitopes during treatment. This indicates that changes during the response to *Mtb* are part of a complex process involving a variety of different epitopes (45) that induce responses from phenotypically diverse T-cell subsets (57), despite well-described immunodominance features. Our results confirm that a major stake in discovering blood-based immune signatures of mycobacterial sterilization lies in finding the appropriate epitopes.

Finally, our study enabled profiling of non-lineage markers. A $CCR4^+CCR6^+$ $CD27^+$ $CD4^+$ EM subset was increased in cured patients compared to pre-treatment, corresponding to a subset enriched in Th17 cells (61, 62). Consistently with previous work on LTBI (63), this suggests that an increase in these cells upon cure might be associated with infection control. Compared to the other $CD4^+$ EM cells, this subset displayed higher CD26 and IL7Ra expression. CD26 participates in T-cell activation and proliferation (64), and correlates with Th1-like responses (65). In parallel, a significant decrease was also observed in an activated $CCR6^+$ $IL7Ra^+$ $CD4^+$ naive subset, which expressed higher levels of CD40L, CD38, and HLA-DR than other $CD4^+$ naive cells. Interestingly, an increase in a $CD4^+$ CM subset which also expressed CD26, IL7Ra, CD27 and CD38 was observed simultaneously. This adds to previous works highlighting a decrease in $CD38^+$ and $HLA\text{-}DR^+$ *Mtb*-specific $CD4^+$ T-cells, including naïve cells, in successfully treated TB patients (9, 10, 13). This suggests that upon TB treatment, differentiated Th17-like $CD4^+$ subsets expressing high levels of CD26 and IL7Ra are enriched in peripheral blood, likely at the expense of less differentiated subsets expressing high levels of CD27 and CD38. Finally, principal components analysis showed that within the subpopulations that differentiated slow from fast converters during treatment, differentiation markers and chemokine receptors contributed to most of the variance, followed by activation and cytotoxicity markers. CD27 and CD26 were among the markers which best discriminated fast and slow responders, consistently with prior studies associating CD27 and CCR4 expression in *Mtb*-specific $CD4^+$ T-cells with active TB compared to latent infection (66). HLA-DR and CD38 also contributed to a lesser extent, which adds to a recent study in which co-expression of CD27, HLA-DR, and CD38 on PPD-stimulated $CD4^+$ T-cells stratified fast and slow responders without restriction to IFN-γ-producing cells (67).

This descriptive study has limitations. The number of patients included was low, resulting in few slow converters, consistently with treated TB course (15 to 20% of slow culture converters). In addition, the presence of within-host *Mtb* isolate micro-diversity has been recently proven in patients treated for DS-TB without culture conversion after two months of well-conducted TB treatment (68), suggesting that it could modulate the host response. We are currently conducting a larger validation study including DS-TB patients only, from whom *Mtb* isolates collected upon treatment initiation and at two months will be screened by whole genome sequencing. In addition, the analyses were not conducted on live cells, but on fixed, cryopreserved peripheral blood cells due to the design of the study using samples collected in lower-income, high TB prevalence settings. For the same reason, the study was conducted on peripheral blood, while the main infectious focus of TB is in the lungs. In addition, since the study required to IGRAs to be performed on the same blood samples prior to cell cryopreservation (24), we did not perform intracellular cytokine staining. Hence, the integrality of the observed cell phenotype changes may not be associated with *Mtb*-specific responses.

However, whether the bulk of anti-TB response relies purely on *Mtb*-specific cells is debated. Given the complexity of the immune response to TB, cellular and molecular interactions are likely to occur between *Mtb*-specific and non-specific subpopulations during mycobacterial clearance, and hence influence the overall T-cell profiles. In addition, the hypothesis that T-cells specific for immunodominant epitopes actually recognize *Mtb*-infected cells has been challenged by studies on mouse models (69), protective immunity post-BCG vaccination (70), and failures of vaccine candidates based on immunodominant antigens (71). In addition, some of the identified cell subpopulations were rare (<1% of $CD3^+$ cells), which is a limitation when using these data for downstream application and studies on implementation in point-of-care tests. However, these subsets enabled identification of biologically meaningful cell phenotype trends that are helpful for target identification.

These limitations are linked to the "bench to bedside" approach adopted in our study. They reflect the reality of the needs for novel TB management tools: accessible samples, simple experimental process, straightforward output. Here, we captured the complexity of T-cell profiles during treatment and narrowed it down to subpopulations of interest associated with cure at the individual level. Mass cytometry does require complex equipment, experiments, and analyses, but we have shown that relevant T-cell profiles could be identified in cryopreserved samples, obtained from small blood volumes, using manual gating analyses and a smaller number of core markers. Future validation studies might confirm the relevancy of simpler phenotypic signatures translatable in primary care settings. Importantly, our study revealed T-cell populations discriminating patient status based on culture conversion, which has a dual impact: on TB management, to better characterize the phenotypes of T-cells involved in TB clearance; and on biomarker research, further supporting that a diversity of epitopes is needed to fully disclose the spectrum of these cells. This work may help identify simpler prognostic biomarkers associated with mycobacterial clearance and the antigens appropriate for their discovery.

DATA AVAILABILITY STATEMENT

The raw data supporting the conclusions of this article will be made available by the authors, without undue reservation.

ETHICS STATEMENT

The studies involving human participants were reviewed and approved by the Institutional Review Board of the National Center for Tuberculosis and Lung Diseases (NCTBLD), Tbilisi, Georgia (IORG0009467) and the Research Review Committee and Ethical Review Committee of the international center for diarrhoeal disease research, Bangladesh (icddr,b) (PR-17076; Version No. 1.3; Version date: 04-01-2018). The patients/participants provided their written informed consent to participate in this study.

AUTHOR CONTRIBUTIONS

FA and JH are the principal investigators and initiated the project together with DG, NT, and SBa. Samples were collected by EK, NT, MU, and SBi. CC and TA designed and optimized the mass cytometry protocol. CC performed all experiments and analyses. CC and FA wrote the manuscript. All authors contributed to the article and approved the submitted version.

FUNDING

This work was supported by Fondation Mérieux, Fondation Christophe et Rodolphe Mérieux, and Fondation AnBer, and the grant ANR-18-CE17-0020. A minor part of the study was supported by the Italian Ministry of Health "Ricerca Corrente, Linea 4".

ACKNOWLEDGMENTS

We would like to thank the patients participating in our study, as well as the healthcare staff and laboratory collaborators in each study site. We would also like to extend our heartfelt thanks to Dr. Marie-Paule Gustin for her kind help with statistical analysis and revisions.

SUPPLEMENTARY MATERIAL

The Supplementary Material for this article can be found online at: https://www.frontiersin.org/articles/10.3389/fimmu.2022.853572/full#supplementary-material

REFERENCES

1. World Health Organization. *Global Tuberculosis Report 2020*. Geneva: WHO Press (2020).
2. World Health Organization. *WHO Consolidated Guidelines on Drug-Resistant Tuberculosis Treatment*. Geneva: WHO Press (2019).
3. World Health Organization. *Global Tuberculosis Report 2018*. Geneva: WHO Press (2018).
4. Singhania A, Verma R, Graham CM, Lee J, Tran T, Richardson M, et al. A Modular Transcriptional Signature Identifies Phenotypic Heterogeneity of Human Tuberculosis Infection. *Nat Commun* (2018) 9:1–17. doi: 10.1038/s41467-018-04579-w
5. Parrish NM, Carroll KC. Role of the Clinical Mycobacteriology Laboratory in Diagnosis and Management of Tuberculosis in Low-Prevalence Settings. *J Clin Microbiol* (2011) 49:772–6. doi: 10.1128/JCM.02451-10
6. Horne DJ, Royce SE, Gooze L, Narita M, Hopewell PC, Nahid P, et al. Sputum Monitoring During Tuberculosis Treatment for Predicting Outcome : Systematic Review and Meta-Analysis. *Lancet Infect Dis* (2010) 10:387–94. doi: 10.1016/S1473-3099(10)70071-2
7. Lienhardt C, Lönnroth K, Menzies D, Balasegaram M, Chakaya J, Cobelens F, et al. Translational Research for Tuberculosis Elimination: Priorities, Challenges, and Actions. *PloS Med* (2016) 13:1–11. doi: 10.1371/journal.pmed.1001965
8. Goletti D, Lindestam Arlehamn CS, Scriba TJ, Anthony R, Maria Cirillo D, Alonzi T, et al. Can We Predict Tuberculosis Cure? Current Tools Available. *Eur Respir J* (2018) 1801089:1–18. doi: 10.1183/13993003.01089-2018
9. Ahmed MIM, Ntinginya NE, Kibiki G, Mtafya BA, Semvua H, Mpagama S, et al. Phenotypic Changes on Mycobacterium Tuberculosis-Specific CD4 T Cells as Surrogate Markers for Tuberculosis Treatment Efficacy. *Front Immunol* (2018) 9:2247. doi: 10.3389/fimmu.2018.02247

10. Adekambi T, Ibegbu CC, Cagle S, Kalokhe AS, Wang YF, Hu Y, et al. Biomarkers on Patient T Cells Diagnose Active Tuberculosis and Monitor Treatment Response (Vol 1252015). *J Clin Invest* (2015) 125:pg 18273723. doi: 10.1172/jci83279
11. Goletti D, Butera O, Bizzoni F, Casetti R, Girardi E, Poccia F. Region of Difference 1 Antigen–Specific CD4 + Memory T Cells Correlate With a Favorable Outcome of Tuberculosis. *J Infect Dis* (2006) 194:984–92. doi: 10.1086/507427
12. Agrawal S, Parkash O, Palaniappan AN, Bhatia AK, Kumar S, Chauhan DS, et al. Efficacy of T Regulatory Cells, Th17 Cells and the Associated Markers in Monitoring Tuberculosis Treatment Response. *Front Immunol* (2018) 9:157. doi: 10.3389/fimmu.2018.00157
13. Riou C, Du Bruyn E, Ruzive S, Goliath RT, Lindestam Arlehamn CS, Sette A, et al. Disease Extent and Anti-Tubercular Treatment Response Correlates With *Mycobacterium Tuberculosis*-Specific CD4 T-Cell Phenotype Regardless of HIV-1 Status. *Clin Transl Immunol* (2020) 9:e1176. doi: 10.1002/cti2.1176
14. Thompson EG, Du Y, Malherbe ST, Shankar S, Braun J, Valvo J, et al. Host Blood RNA Signatures Predict the Outcome of Tuberculosis Treatment. *Tuberculosis* (2017) 107:48–58. doi: 10.1016/j.tube.2017.08.004
15. Zak DE, Penn-Nicholson A, Scriba TJ, Thompson E, Suliman S, Amon LM, et al. A Blood RNA Signature for Tuberculosis Disease Risk: A Prospective Cohort Study. *Lancet* (2016) 387:2312–22. doi: 10.1016/S0140-6736(15)01316-1
16. Scriba TJ, Fiore-Gartland A, Penn-Nicholson A, Mulenga H, Kimbung Mbandi S, Borate B, et al. Biomarker-Guided Tuberculosis Preventive Therapy (CORTIS): A Randomised Controlled Trial. *Lancet Infect Dis* (2021) 21:354–65. doi: 10.1016/S1473-3099(20)30914-2
17. Chiacchio T, Delogu G, Vanini V, Cuzzi G, DE Maio F, Pinnetti C, et al. Immune Characterization of the HBHA-Specific Response in Mycobacterium Tuberculosis-Infected Patients With or Without HIV Infection. *PloS One* (2017) 12:1–18. doi: 10.1371/journal.pone.0183846
18. Musvosvi M, Duffy D, Filander E, Africa H, Mabwe S, Jaxa L, et al. T-Cell Biomarkers for Diagnosis of Tuberculosis: Candidate Evaluation by a Simple Whole Blood Assay for Clinical. *Eur Respir J* (2018) 51:1–4. doi: 10.1183/13993003.00153-2018
19. Gossez M, Rimmelé T, Andrieu T, Debord S, Bayle F, Malcus C, et al. Proof of Concept Study of Mass Cytometry in Septic Shock Patients Reveals Novel Immune Alterations. *Sci Rep* (2018) 8:1–12. doi: 10.1038/s41598-018-35932-0
20. Kourelis TV, Villasboas JC, Jessen E, Dasari S, Dispenzieri A, Jevremovic D. Mass Cytometry Dissects T Cell Heterogeneity in the Immune Tumor Microenvironment of Common Dysproteinemias at Diagnosis and After Fi Rst Line Therapies. *Blood Cancer J* (2019) 9:1–13. doi: 10.1038/s41408-019-0234-4
21. Rubin SJS, Bai L, Haileselassie Y, Garay G, Yun C, Becker L, et al. Mass Cytometry Reveals Systemic and Local Immune Signatures That Distinguish Inflammatory Bowel Diseases. *Nat Commun* (2019) 10:1–14. doi: 10.1038/s41467-019-10387-7
22. Roy Chowdhury R, Vallania F, Yang Q, Lopez Angel CJ, Darboe F, Penn-Nicholson A, et al. A Multi-Cohort Study of the Immune Factors Associated With M. Tuberculosis Infection Outcomes. *Nature* (2018) 560:644–8. doi: 10.1038/s41586-018-0439-x
23. Chedid C, Kokhreidze E, Tukvadze N, Banu S, Uddin MKM, Biswas S, et al. Association of Baseline White Blood Cell Counts With Tuberculosis Treatment Outcome: A Prospective Multicentered Cohort Study. *Int J Infect Dis* (2020) 100:199–206. doi: 10.1016/j.ijid.2020.09.017
24. Chedid C, Kokhreidze E, Tukvadze N, Banu S, Uddin MKM, Biswas S, et al. Relevance of QuantiFERON-TB Gold Plus and Heparin-Binding Hemagglutinin Interferon-γ Release Assays for Monitoring of Pulmonary Tuberculosis Clearance: A Multicentered Study. *Front Immunol* (2021) 11:616450. doi: 10.3389/fimmu.2020.616450
25. Petruccioli E, Chiacchio T, Pepponi I, Vanini V, Urso R, Cuzzi G, et al. First Characterization of the CD4 and CD8 T-Cell Responses to QuantiFERON-TB Plus. *J Infect* (2016) 73:588–97. doi: 10.1016/j.jinf.2016.09.008
26. *Qiagen. QuantiFERON®-TB Gold Plus (QFT®-Plus) Package Insert*, Vol. 96. Germantown, MD, USA: Qiagen (2017). p. 1101062. doi: 10.1016/j.athoracsur.2015.08.092.
27. Delogu G, Chiacchio T, Vanini V, Butera O, Cuzzi G, Bua A, et al. Methylated HBHA Produced in M. Smegmatis Discriminates Between Active and non-Active Tuberculosis Disease Among RD1-Responders. *PloS One* (2011) 6:1–8. doi: 10.1371/journal.pone.0018315
28. Rahman AH, Tordesillas L, Berin MC. Heparin Reduces Nonspecific Eosinophil Staining Artifacts in Mass Cytometry Experiments. *Cytometry* (2016) 89A:601–7. doi: 10.1002/cyto.a.22826
29. Mei HE, Leipold MD, Schulz AR, Chester C, Maecker HT. Barcoding of Live Human Peripheral Blood Mononuclear Cells for Multiplexed Mass Cytometry. *J Immunol* (2015) 194:2022–31. doi: 10.4049/jimmunol.1402661
30. Leipold MD, Newell EW, Maecker HT. Multiparameter Phenotyping of Human PBMCs Using Mass Cytometry. *Methods Mol Biol* (2015) 1343:1–14. doi: 10.1007/978-1-4939-2963-4
31. McGuire HM, Ashhurst TM. *Mass Cytometry: Methods and Protocols*. New York: Springer (2019). Available at: https://books.google.co.uk/books?id=fvjTwQEACAAJ.
32. Becht E, McInnes L, Healy J, Dutertre CA, Kwok IWH, Ng LG, et al. Dimensionality Reduction for Visualizing Single-Cell Data Using UMAP. *Nat Biotechnol* (2019) 37:38–47. doi: 10.1038/nbt.4314
33. Ashhurst TM, Marsh-Wakefield F, Putri GH, Spiteri AG, Shinko D, Read MN, et al. Integration, Exploration, and Analysis of High-Dimensional Single-Cell Cytometry Data Using Spectre. *Cytometry Part A* (2022) 101(3):237–53. doi: 10.1002/cyto.a.24350
34. Van Gassen S, Callebaut B, Van Helden MJ, Lambrecht BN, Demeester P, Dhaene T, et al. FlowSOM: Using Self-Organizing Maps for Visualization and Interpretation of Cytometry Data. *Cytom Part A* (2015) 87:636–45. doi: 10.1002/cyto.a.22625
35. Quintelier K, Couckuyt A, Emmaneel A, Aerts J, Saeys Y, Van Gassen S. Analyzing High-Dimensional Cytometry Data Using FlowSOM. *Nat Protoc* (2021) 16:3775–801. doi: 10.1038/s41596-021-00550-0
36. Pereira DG, Afonso A, Medeiros FM. Overview of Friedmans Test and *Post-Hoc* Analysis. *Commun Stat Simul Comput* (2015) 44:2636–53. doi: 10.1080/03610918.2014.931971
37. Yoav B, Yosef H. Controlling the False Discovery Rate: A Practical and Powerful Approach to Multiple Testing. *J R Stat Soc Ser B* (1995) 57:289–300. doi: 10.1111/j.2517-6161.1995.tb02031.x
38. Althouse AD. Adjust for Multiple Comparisons? It's Not That Simple. *Ann Thorac Surg* (2016) 101:1644–5. doi: 10.1016/j.athoracsur.2015.11.024
39. Marriott I, Stephens R, Serrano CJ, Gennaro ML, Arrigucci R, Lakehal K, et al. Active Tuberculosis Is Characterized by Highly Differentiated Effector Memory Th1 Cells. *Front Immunol* (2018) 9:2127. doi: 10.3389/fimmu.2018.02127
40. Chiacchio T, Petruccioli E, Vanini V, Cuzzi G, Pinnetti C, Sampaolesi A, et al. Polyfunctional T-Cells and Effector Memory Phenotype are Associated With Active TB in HIV-Infected Patients. *J Infect* (2014) 69:533–45. doi: 10.1016/j.jinf.2014.06.009
41. Wang X, Cao Z, Jiang J, Niu H, Dong M, Tong A, et al. Association of Mycobacterial Antigen-Specific CD4+ Memory T Cell Subsets With Outcome of Pulmonary Tuberculosis. *J Infect* (2010) 60:133–9. doi: 10.1016/j.jinf.2009.10.048
42. Petruccioli E, Petrone L, Vanini V, Sampaolesi A, Gualano G, Girardi E, et al. Ifnγ/Tnfα Specific-Cells and Effector Memory Phenotype Associate With Active Tuberculosis. *J Infect* (2013) 66:475–86. doi: 10.1016/j.jinf.2013.02.004
43. Goletti D, Butera O, Bizzoni F, Casetti R, Giradi E, Poccia F. Region of Difference 1 Antigen-Specific CD4+ Memory T Cells Correlate With a Favorable Outcome of Tuberculosis. *J Infect Dis* (2006) 194:984–92. doi: 10.1086/507427
44. Nyendak MR, Park B, Null MD, Baseke J, Swarbrick G, Mayanja-Kizza H, et al. Mycobacterium Tuberculosis Specific CD8+ T Cells Rapidly Decline With Antituberculosis Treatment. *PloS One* (2013) 8:133–9. doi: 10.1371/journal.pone.0081564
45. Axelsson-Robertson R, Rao M, Loxton AG, Walzl G, Bates M, Zumla A, et al. Frequency of Mycobacterium Tuberculosis-Specific CD8+ T-Cells in the Course of Anti-Tuberculosis Treatment. *Int J Infect Dis* (2015) 32:23–9. doi: 10.1016/j.ijid.2015.01.017
46. Riou C, Gray CM, Lugongolo M, Gwala T, Kiravu A, Deniso P, et al. A Subset of Circulating Blood Mycobacteria-Specific CD4 T Cells can Predict the Time to Mycobacterium Tuberculosis Sputum Culture Conversion. *PloS One* (2014) 9:1–11. doi: 10.1371/journal.pone.0102178
47. Lewinsohn DA, Swarbrick GM, Park B, Cansler ME, Null MD, Toren KG, et al. Comprehensive Definition of Human Immunodominant CD8 Antigens in Tuberculosis. *NPJ Vaccines* (2017) 2:1–10. doi: 10.1038/s41541-017-0008-6

48. Chiacchio T, Petruccioli E, Vanini V, Cuzzi G, La Manna MP, Orlando V, et al. Impact of Antiretroviral and Tuberculosis Therapies on CD4+ and CD8 + HIV/M. Tuberculosis-Specific T-Cell in Co-Infected Subjects. *Immunol Lett* (2018) 198:33–43. doi: 10.1016/j.imlet.2018.04.001
49. Serbina NV, Liu C-C, Scanga CA, Flynn JL. CD8+ CTL From Lungs of Mycobacterium Tuberculosis -Infected Mice Express Perforin *In Vivo* and Lyse Infected Macrophages. *J Immunol* (2000) 165:353–63. doi: 10.4049/jimmunol.165.1.353
50. Lin PL, Flynn JL. CD8 T Cells and Mycobacterium Tuberculosis Infection. *Semin Immunopathol* (2015) 37:239–49. doi: 10.1007/s00281-015-0490-8
51. Bruns H, Meinken C, Schauenberg P, Härter G, Kern P, Modlin RL, et al. Anti-TNF Immunotherapy Reduces CD8+ T Cell–Mediated Antimicrobial Activity Against Mycobacterium Tuberculosis in Humans. *JCI* (2009) 119:1167–77. doi: 10.1172/JCI38482.ated
52. Jiang HB, Gong HL, Zhang Q, Gu J, Liang L, Zhang J. Decreased Expression of Perforin in CD8(+) T Lymphocytes in Patients With Mycobacterium Tuberculosis Infection and its Potential Value as a Marker for Efficacy of Treatment. *J Thorac Dis* (2017) 9:1353–+. doi: 10.21037/jtd.2017.05.74
53. Rozot V, Vigano S, Mazza-stalder J, Idrizi E, Day CL, Perreau M, et al. Mycobacterium Tuberculosis-Specific CD8+ T Cells are Functionally and Phenotypically Different Between Latent Infection and Active Disease. *Eur J Immunol* (2013) 43:1568–77. doi: 10.1002/eji.201243262.Mycobacterium
54. Durward M, Radhakrishnan G, Harms J, Bareiss C, Magnani D, Splitter GA. Active Evasion of CTL Mediated Killing and Low Quality Responding CD8+ T Cells Contribute to Persistence of Brucellosis. *PloS One* (2012) 7:1–16. doi: 10.1371/journal.pone.0034925
55. Riou C, Berkowitz N, Goliath R, Burgers WA, Wilkinson RJ. Analysis of the Phenotype of Mycobacterium Tuberculosis-Specific CD4+ T Cells to Discriminate Latent From Active Tuberculosis in HIV-Uninfected and HIV-Infected Individuals. *Front Immunol* (2017) 8:968. doi: 10.3389/fimmu.2017.00968
56. Grotzke JE, Lewinsohn DM. Role of CD8+ T Lymphocytes in Control of Mycobacterium Tuberculosis Infection. *Microbes Infect* (2005) 7:776–88. doi: 10.1016/j.micinf.2005.03.001
57. Axelsson-Robertson R, Ju JH, Kim HY, Zumla A, Maeurer M. Mycobacterium Tuberculosis-Specific and MHC Class I-Restricted CD8+ T-Cells Exhibit a Stem Cell Precursor-Like Phenotype in Patients With Active Pulmonary Tuberculosis. *Int J Infect Dis* (2015) 32:13–22. doi: 10.1016/j.ijid.2014.12.017
58. Masungi C, Temmerman S, Van Vooren JP, Drowart A, Pethe K, Menozzi FD, et al. Differential T and B Cell Responses Against Mycobacterium Tuberculosis Heparin-Binding Hemagglutinin Adhesin in Infected Healthy Individuals and Patients With Tuberculosis. *J Infect Dis* (2002) 185:513–20. doi: 10.1086/338833
59. Sali M, Buonsenso D, D'Alfonso P, De Maio F, Ceccarelli M, Battah B, et al. Quantiferon and HBHA-Based IGRA Supports Tuberculosis Diagnosis and Therapy Management in Children. *J Infect* (2018):526–33. doi: 10.1016/j.jinf.2018.09.011
60. De Maio F, Squeglia F, Goletti D, Delogu G. The Mycobacterial HBHA Protein: A Promising Biomarker for Tuberculosis. *Curr Med Chem* (2018) 26:2051–60. doi: 10.2174/0929867325666181029165805
61. Kim CH, Rott L, Kunkel EJ, Genovese MC, Andrew DP, Wu L, et al. Rules of Chemokine Receptor Association With T Cell Polarization. *Vivo J Clin Invest* (2001) 108:1331–9. doi: 10.1172/JCI13543
62. Acosta-Rodriguez EV, Rivino L, Geginat J, Jarrossay D, Gattorno M, Lanzavecchia A, et al. Surface Phenotype and Antigenic Specificity of Human Interleukin 17-Producing T Helper Memory Cells. *Nat Immunol* (2007) 8:639–46. doi: 10.1038/ni1467
63. Lindestam Arlehamn CS, Gerasimova A, Mele F, Henderson R, Swann J, Greenbaum JA, et al. Memory T Cells in Latent Mycobacterium Tuberculosis Infection Are Directed Against Three Antigenic Islands and Largely Contained in a CXCR3+CCR6+ Th1 Subset. *PloS Pathog* (2013) 9:1–14. doi: 10.1371/journal.ppat.1003130
64. Klemann C, Wagner L, Stephan M, von Hörsten S. Cut to the Chase: A Review of CD26/dipeptidyl Peptidase-4's (DPP4) Entanglement in the Immune System. *Clin Exp Immunol* (2016) 185:1–21. doi: 10.1111/cei.12781
65. Ohnuma K, Dang NH, Morimoto C. Revisiting an Old Acquaintance: CD26 and its Molecular Mechanisms in T Cell Function. *Trends Immunol* (2008) 29:295–301. doi: 10.1016/j.it.2008.02.010
66. Latorre I, Fernández-Sanmartín MA, Muriel-Moreno B, Villar-Hernández R, Vila S, De Souza-Galvão ML, et al. Study of CD27 and CCR4 Markers on Specific CD4+ T-Cells as Immune Tools for Active and Latent Tuberculosis Management. *Front Immunol* (2019) 9:3094. doi: 10.3389/fimmu.2018.03094
67. Vickers MA, Darboe F, Muefong CN, Mbayo G, Barry A, Gindeh A, et al. Monitoring Anti-Tuberculosis Treatment Response Using Analysis of Whole Blood Mycobacterium Tuberculosis Specific T Cell Activation and Functional Markers. *Front Immunol* (2020) 11:572620. doi: 10.3389/fimmu.2020.572620
68. Genestet C, Hodille E, Barbry A, Berland J-L, Hoffmann J, Westeel E, et al. Rifampicin Exposure Reveals Within-Host Mycobacterium Tuberculosis Diversity in Patients With Delayed Culture Conversion. *PloS Pathog* (2021) 17:e1009643. doi: 10.1371/journal.ppat.1009643
69. Patankar YR, Sutiwisesak R, Boyce S, Lai R, Lindestam Arlehamn CS, Sette A, et al. Limited Recognition of Mycobacterium Tuberculosis-Infected Macrophages by Polyclonal CD4 and CD8 T Cells From the Lungs of Infected Mice. *Mucosal Immunol* (2020) 13:140–8. doi: 10.1038/s41385-019-0217-6
70. Kagina BMN, Abel B, Scriba TJ, Hughes EJ, Keyser A, Soares A, et al. Specific T Cell Frequency and Cytokine Expression Profile do Not Correlate With Protection Against Tuberculosis After Bacillus Calmette-Guérin Vaccination of Newborns. *Am J Respir Crit Care Med* (2010) 182:1073–9. doi: 10.1164/rccm.201003-0334OC
71. Moguche AO, Musvosvi M, Penn-Nicholson A, Plumlee CR, Mearns H, Geldenhuys H, et al. Antigen Availability Shapes T Cell Differentiation and Function During Tuberculosis. *Cell Host Microbe* (2017) 21:695–706.e5. doi: 10.1016/j.chom.2017.05.012

Conflict of Interest: DG reports personal fees from Biomérieux (consulting), Qiagen (consulting, lectures), and Diasorin (lectures) outside the submitted work.

The remaining authors declare that the research was conducted in the absence of any commercial or financial relationships that could be construed as a potential conflict of interest.

Publisher's Note: All claims expressed in this article are solely those of the authors and do not necessarily represent those of their affiliated organizations, or those of the publisher, the editors and the reviewers. Any product that may be evaluated in this article, or claim that may be made by its manufacturer, is not guaranteed or endorsed by the publisher.

Copyright © 2022 Chedid, Andrieu, Kokhreidze, Tukvadze, Biswas, Ather, Uddin, Banu, De Maio, Delogu, Endtz, Goletti, Vocanson, Dumitrescu, Hoffmann and Ader. This is an open-access article distributed under the terms of the Creative Commons Attribution License (CC BY). The use, distribution or reproduction in other forums is permitted, provided the original author(s) and the copyright owner(s) are credited and that the original publication in this journal is cited, in accordance with accepted academic practice. No use, distribution or reproduction is permitted which does not comply with these terms.